Original Article

A virtual joint method of analytical form for parallel manipulators

Hui Zhang[1,2], Zhenbang Xu[1,3], Hasiaoqier Han[1] (ID), Chunyang Han[1], Yang Yu[1] and Mingyi Xia[1]

Abstract

Oriented towards the stiffness optimization of parallel manipulators, a stiffness modeling method based on subspace analysis was proposed. The paper revealed the "shielding effect" of passive joints, i.e. shielding the partial local stiffness of a mechanism on Cartesian space, and accordingly brought forward the concept of Effective Stiffness Tensor (EST), which was then obtained by introducing the orthogonal projector. The method allows a stiffness model of analytical form as well as high computation efficiency, which makes it suitable for applications in the stiffness optimization of parallel manipulators. Proposed method had been applied to the parallel alignment mechanism in China's large space telescope and verified by dynamic experiments.

Introduction

Parallel manipulators are widely used in aerospace, precision machine tools and other fields[1–5] and configuration parameter optimization is indispensable to make the stiffness performance meet engineering demands. Therefore, an accurate and efficient stiffness model of parallel manipulators is fundamental.

The finite element method (FEM) has been widely used in stiffness analysis since its potential of accurately describing the stiffness characteristics of manipulators. However, the great modeling complexity, heavy computational burden and low model portability also hinder its application in design. Therefore, many efficient modelling methods were proposed as supplements. In the field of compliant mechanism, free-body-diagram (FBD) based modelling approach is one of the main methods and constraint-force-based (CFB) approach[6] is one of its fruitful developments. As for traditional manipulators, matrix structure analysis (MSA) and virtual-joint method (VJM) were proposed. MSA was developed on the basis of the FEM using large structural elements such as beams, arcs and cables to describe the mechanical characteristics of components. A remarkable feature of MSA is that it allows the convenient analysis of manipulators of complex topology.[7] Hence, the Cartesian space stiffness matrices of complex parallel manipulators are simply obtained following general steps by MSA.[7–10] However, MSA has a disadvantage that it has a heavy calculation burden of the inversion of a matrix with high dimension. Klimchik compared calculation complexity of several methods measured by the number of floating-point operations, and concluded that the calculation complexity of the MSA was on the order of 10^7–10^8 in the analysis of three types of parallel manipulators while that of the VJM was only on the order of 10^3 with comparable precision.[11] On the other hand, it's cumbersome for an MSA model to handle manipulators with multiple passive joints, which made it barely applied to configuration optimization.[7]

VJM is based on the idea of approximating structure deformation with the joint motion that is similar

[1]CAS Key Laboratory of On-orbit Manufacturing and Integration for Space Optics System, Changchun Institute of Optics, Fine Mechanics and Physics, Chinese Academy of Sciences, Changchun, China
[2]University of Chinese Academy of Sciences, Beijing, China
[3]Center of Materials Science and Optoelectronics Engineering, University of Chinese Academy of Sciences, Beijing, China

Corresponding author:
Zhenbang Xu, CAS Key Laboratory of On-orbit Manufacturing and Integration for Space Optics System, Changchun Institute of Optics, Fine Mechanics and Physics, Chinese Academy of Sciences, No. 3888 Dong Nanhu Road, Changchun 130033, China.
Email: xuzhenbang@ciomp.ac.cn

to pseudo-rigid-body model (PRBM). However, VJM was originally aiming for stiffness modeling of traditional mechanisms and thus significantly different from PRBM about key problems and mathematical methods eventually. The VJM was first proposed by Salisbury[12] and Gosselin,[13] in which the equation (i.e., the conservative congruence transformation) for calculating the holistic stiffness that described by Cartesian space compliance matrix of manipulators was obtained after the joint space compliance matrix was defined to describe the local compliance distribution of manipulators. In follow-up studies, the compliance of links was also considered and equated to joint compliance to improve the accuracy of the models,[14] and virtual joints with elastic characteristics in multiple directions[15–17] were adopted to describe the more complex deformation behavior of the structure as a complement of virtual joints of a single degree of freedom (DOF) used in early works.[18] A key problem of the VJM using virtual joints with multiple DOF is how to obtain all the elastic parameters of the joints. At first, researchers used a simple cantilever beam to estimate the elastic characteristics of the structure, which provided a rough approximation.[15,16] Klimchik et al. then proposed parameter identification method based on the finite element and a practical identification method,[19–23] which simplified the process of parameter estimation and greatly improved the precision of the VJM.

There are many research works about the application of VJM in parallel manipulators[11,24–27] since it is very convenient to integrate configuration parameters into a VJM model with smaller computational burden than FEM and MSA. However, the current method need to obtain a partition of the inversion of a dimension-extended compliance matrix,[11,27–29] which couldn't directly provide a stiffness formula of the analytical and explicit form and thus unnecessarily introduces numeric iteration computation. The analytical model could be obtained if there were proper constraints on virtual joints, for example, the forms of virtual joints are complete same as actuators.[30–32] However, inadequate virtual joints would hinder the application in optimization. Specifically, if the model neglected the deformation of passive joints and links and so on, the influence of corresponding parameters on holistic stiffness would also deviate from the real effect and then it would be difficult to apply the models to comprehensive optimization of configuration parameters.

To this end, the present paper introduced a stiffness modeling method for parallel manipulators based on subspace analysis. From the perspective of linear space, the method revealed that of passive joints would shield partial local stiffness on Cartesian space and accordingly brought forward the concept of EST, which was then obtained by introducing the orthogonal projector. The method provides a stiffness model of analytical and explicit

form and thus allows direct computation and high efficiency. Meanwhile, by introducing the projectors, the method also provides an open solution framework that is compatible with the more number of efficient algebraic tools. Proposed method had been applied to the parallel alignment manipulator in China's large space telescope.

The remainder of the paper was organized as following. The upcoming section presented the modified method. Next section introduced application of the proposed method in the prototype of alignment mechanism and corresponding validity experiments. The last section summarized the contents and contributions of the paper.

The modified virtual joint method of a parallel manipulators

VJM formulas and requirements of optimization model

For a general manipulator, the deformations of the structures have also the impact on the manipulator stiffness, such as the links, guides and so on. The basic idea of VJM is to assume that the deformation inside manipulators is completely concentrated on some virtual joints and restore the motion and mechanical characteristic of the local deformation by these virtual joints. As a result, the stiffness characteristic of manipulators can be completely described by elastic joints.

The elastic joints on a manipulator always produce resistance when they move. Due to the limit for practical allowable stress of traditional manipulators, the local deformation considered in VJM is always tiny. The basic assumption allows using Jacobian to describe the relationship between local deformation and motion of virtual joints as well as the relationship between the external load newly added and local deformation newly occurring. Therefore, the relationship between variations of joint movement and those of their resistance can be always expressed in a linear form

$$\delta\vec{\vartheta}_j = \mathbf{C}_{\vartheta j}\delta\vec{w}_j, \quad (j=1,\ldots,N) \tag{1}$$

or

$$\delta\vec{\vartheta} = \begin{pmatrix} \delta\vec{\vartheta}_1 \\ \vdots \\ \delta\vec{\vartheta}_N \end{pmatrix} = \begin{bmatrix} \mathbf{C}_{\vartheta 1} & & \\ & \ddots & \\ & & \mathbf{C}_{\vartheta N} \end{bmatrix} \begin{pmatrix} \delta\vec{w}_1 \\ \vdots \\ \delta\vec{w}_N \end{pmatrix}$$
$$= \mathbf{C}_{\vartheta}\delta\vec{w} \tag{2}$$

where $\vec{\vartheta}_j$ and $\vec{w}_j$ respectively represent the joint variable vector in the j-th elastic joint and the corresponding resistance vector, and $\mathbf{C}_{\vartheta j}$ and $\mathbf{C}_{\vartheta}$ are

respectively the compliance matrix of the j-th joint and joint space compliance matrix, and $\delta(\cdot)$ represents the variation of a variable, and N is the total number of elastic joints. Due to the linear expressions, the positions of virtual joints are arbitrary on the local structures and usually arranged in the nearby physical joints. As a result, the positions of virtual joints relative to local structures keep unchanged and local structures could be considered rigid.

Denote the motion Jacobian matrix of elastic joints as $\mathbf{J}_\vartheta$ and that of passive joints as $\mathbf{J}_\eta$, and the variations of the end-effector Cartesian coordinates satisfy

$$\delta\vec{q} = \mathbf{J}_\vartheta\delta\vec{\vartheta} + \mathbf{J}_\eta\delta\vec{\eta} \tag{3}$$

where $\vec{\eta}$ is the vector consisting of joint variables of passive joints, and $\vec{q}$ represents Cartesian coordinates of the end-effector. There is not a definite relationship between the motion of passive joints and the external load and thus the motion of passive joints kinematically depends on that of elastic joints, so $\delta\vec{\eta}$ is always capable to be expressed as

$$\delta\vec{\eta} = G_{\eta\vartheta}\delta\vec{\vartheta} \tag{4}$$

where $G_{\eta\vartheta}$ represents the constraint Jacobian matrix. Therefore, we have

$$\delta\vec{q} = (\mathbf{J}_\vartheta + \mathbf{J}_\eta G_{\eta\vartheta})\delta\vec{\vartheta} = N\delta\vec{\vartheta} \tag{5}$$

According to the principle of virtual work, the virtual work done by external wrench $\vec{t}$ satisfies

$$\delta W = \vec{t}^{\mathrm{T}}\delta\vec{q} = \vec{w}_\vartheta^{\mathrm{T}}\delta\vec{\vartheta} + \vec{w}_\eta^{\mathrm{T}}\delta\vec{\eta} \tag{6}$$

where $\vec{w}_\vartheta$ and $\vec{w}_\eta$ respectively represents the deformation resistance of elastic joints and the force in passive joints. Recalling equation (4) and (5) and the equation is simplified as

$$\vec{t}^{\mathrm{T}}N\delta\vec{\vartheta} = \left(\vec{w}_\vartheta^{\mathrm{T}} + \vec{w}_\eta^{\mathrm{T}}G_{\eta\vartheta}\right)\delta\vec{\vartheta} \tag{7}$$

As a result, the relationship between $\vec{w}_\vartheta$ and $\vec{t}$ is

$$\vec{w}_\vartheta = N^{\mathrm{T}}\vec{t} - G_{\eta\vartheta}^{\mathrm{T}}\vec{w}_\eta \tag{8}$$

Recalling equations (2), (5) and (8), and the relationship between resultant displacement and external wrench is

$$\delta\vec{q} = \left(\vec{t}^{\mathrm{T}} \otimes NC_\vartheta\right)\delta\left(\mathrm{vec}(N^{\mathrm{T}})\right) \\ - \left(\vec{w}_\eta^{\mathrm{T}} \otimes NC_\vartheta\right)\delta\left(\mathrm{vec}\left(G_{\eta\vartheta}^{\mathrm{T}}\right)\right) \\ + NC_\vartheta N^{\mathrm{T}}\delta\vec{t} - NC_\vartheta G_{\eta\vartheta}^{\mathrm{T}}\delta\vec{w}_\eta \tag{9}$$

where symbol "$\otimes$" and "vec$(\cdot)$" respectively denote the Kronecker product and vectorizing operator. In addition, the variation of vector $\mathrm{vec}(N^T)$ and $\mathrm{vec}\left(G_{\eta\vartheta}^{\mathrm{T}}\right)$ can be expressed as:

$$\delta\left(\mathrm{vec}(N^{\mathrm{T}})\right) = \frac{\partial\mathrm{vec}(N^{\mathrm{T}})}{\partial\vec{q}^{\mathrm{T}}}\delta\vec{q} = \mathbf{H}_N\delta\vec{q} \tag{10}$$

$$\delta\left(\mathrm{vec}\left(G_{\eta\vartheta}^{\mathrm{T}}\right)\right) = \frac{\partial\mathrm{vec}\left(G_{\eta\vartheta}^{\mathrm{T}}\right)}{\partial\vec{q}^{\mathrm{T}}}\delta\vec{q} = \mathbf{H}_G\delta\vec{q} \tag{11}$$

and thus we have the relationship between external wrench and the resultant displacement of Cartesian coordinates

$$\delta\vec{q} = \mathbf{A}\left(NC_\vartheta N^{\mathrm{T}}\delta\vec{t} - NC_\vartheta G_{\eta\vartheta}^{\mathrm{T}}\delta\vec{w}_\eta\right) \tag{12}$$

where

$$\mathbf{A} = \left[\mathbf{I}_6 - \left(\vec{t}^{\mathrm{T}} \otimes NC_\vartheta\right)\mathbf{H}_N - \left(\vec{w}_\eta^{\mathrm{T}} \otimes NC_\vartheta\right)\mathbf{H}_G\right]^{-1} \tag{13}$$

It is seen that holistic mechanical characteristics of manipulators may vary with the external load due to the existence of passive joints even the mechanical characteristics of local structures remain linear.

All the Jacobian matrix in the formula can be considered constant in holistic stiffness optimization since the concerned stiffness frees from how the deformation process of a manipulator would be. In addition, the optimization targets at improving the intrinsic attributes and thus is not interested in the influence of external factors on the manipulator stiffness. Specifically, the external wrench on the manipulator would be considered constant, and the non-perfect factors such as dead zones, saturation, force in passive joints and so on would be neglected because their effect on stiffness would be sensitive to the change of the external wrench and hard to estimate. In fact, the non-perfect factors are avoided in practice as much as possible and thus their influences on the manipulator performance are always weak. As a result, the compliance model for optimization is expressed as

$$\mathbf{C}_c = \left[\mathbf{I}_6 - \left(\vec{t}^{\mathrm{T}} \otimes NC_\vartheta\right)\mathbf{H}_N\right]^{-1} \\ \times (\mathbf{J}_\vartheta + \mathbf{J}_\eta G_{\eta\vartheta})\mathbf{C}_\vartheta(\mathbf{J}_\vartheta + \mathbf{J}_\eta G_{\eta\vartheta})^{\mathrm{T}} \tag{14}$$

Taking the internal stress and preload on the manipulator as zeros, the formula of the Cartesian space compliance matrix could be further simplified

and we get what is so called Conservative Congruence Transformation (CCT)

$$\mathbf{C}_c = N\mathbf{C}_\vartheta N^{\mathrm{T}} = (\mathbf{J}_\vartheta + \mathbf{J}_\eta G_{\eta\vartheta})\mathbf{C}_\vartheta(\mathbf{J}_\vartheta + \mathbf{J}_\eta G_{\eta\vartheta})^{\mathrm{T}}$$
(15)

It is important for the stiffness model to have an analytical form and high computational efficiency. The computational burden of the stiffness model is of significance to the optimization efficiency since there are always many iteration steps during the optimization process and the computation of the stiffness model would be performed at every step. Stiffness formulas of analytical forms would also be beneficial since they allow more types of optimization algorithms, especially those of high efficiency, which would be fundamental to reduce the iteration steps on the condition that there are many parameters to be optimized.

VJM based on the subspace analysis

It would be difficult to integrate multiple virtual joints into a VJM model through mere kinematic methods since the manipulators with redundant DOF of virtual joints would be kinematically indeterminate. Hence, an additional mechanics method is necessary. According to the principle of superposition, the resistance wrench of a parallel manipulator is the sum of that of each serial branch chain

$$\mathbf{K}_M\delta\vec{q} = \vec{t} = \sum_{i=1}^{n}\vec{\tau}_i = \sum_{i=1}^{n}\mathbf{K}_i\delta\vec{q}$$
(16)

where $\vec{t}$ and $\mathbf{K}_M$ respectively represent the resistance wrench and stiffness of the parallel manipulator and $\vec{\tau}_i$ and $\mathbf{K}_i$ respectively represent the those of the i-th branch chain, and n represents the number of branch chains. As a result, the equivalent problem is to solve the stiffness of several serial chains, as is shown in

Figure 1. Considering that there are always forward motion Jacobian (i.e., $\mathbf{J}_\vartheta$ and $\mathbf{J}_\eta$) of explicit and analytical form for a serial kinematic chain, all that is left is constraint matrix (i.e., $G_{\eta\vartheta}$) of each chain, which would be obtained by the method based on subspace analysis in this subsection.

Denote the linear space of Cartesian coordinates as Ω_C and linear space of elastic joint variables of the i-th branch chain as $\Omega_{\vartheta i}$, and it's natural that joint space compliance matrix $\mathbf{C}_{\vartheta i}$ is a symmetric second-order tensor on $\Omega_{\vartheta i}$, and CCT is a linear transformation of second-order tensor in essence from the perspective of tensor analysis, which depends on how the elements on $\Omega_{\vartheta i}$ are mapped to those on $\Omega_{\vartheta i}$. In other words, as long as the linear transformation of vectors is determined, the CCT is consequently obtained. For a branch chain without passive joints, the motion of the end-effector is completely decided by that of elastic joints and thus the vector transformation is exactly the motion Jacobian matrix of elastic joints $\mathbf{J}_{\vartheta i}$, at which the local compliance attributes described by $\mathbf{C}_{\vartheta i}$ are completely projected onto holistic space Ω_C. However, it would be different when it comes to a branch chain with passive joints and specifically, the passive joints would partly "shield" the linear transformation that projects the compliance.

Considering the i-th serial branch chain with passive joints, any permissible wrench on the end-effector of the chain must ensure that the work done to passive joints keeps zero in order to make it possible that the serial branch is in static equilibrium, i.e.,

$$\vec{w}_{\eta i}^{\mathrm{T}}\delta\vec{\eta}_i = 0, \ \forall\delta\vec{\eta}_i \in \Omega_{\eta i}$$
$$\Longrightarrow \vec{\tau}_i^{\mathrm{T}}\mathbf{J}_{F\eta i}^{\mathrm{T}}\delta\vec{\eta}_i = \vec{\tau}_i^{\mathrm{T}}\mathbf{J}_{\eta i}\delta\vec{\eta}_i = \vec{\tau}_i^{\mathrm{T}}\delta\vec{q} = 0, \ \forall\delta\vec{q} \in \Omega_{C\eta i}$$
(17)

where $\Omega_{\eta i}$ denotes the linear space of passive joint variables $\vec{\eta}_i$, and $\Omega_{C\eta i}$ represents the subspace of Ω_C and also the codomain of linear transformation $\mathbf{J}_{\eta i}$, whose domain is $\Omega_{\eta i}$ and transposition is the force
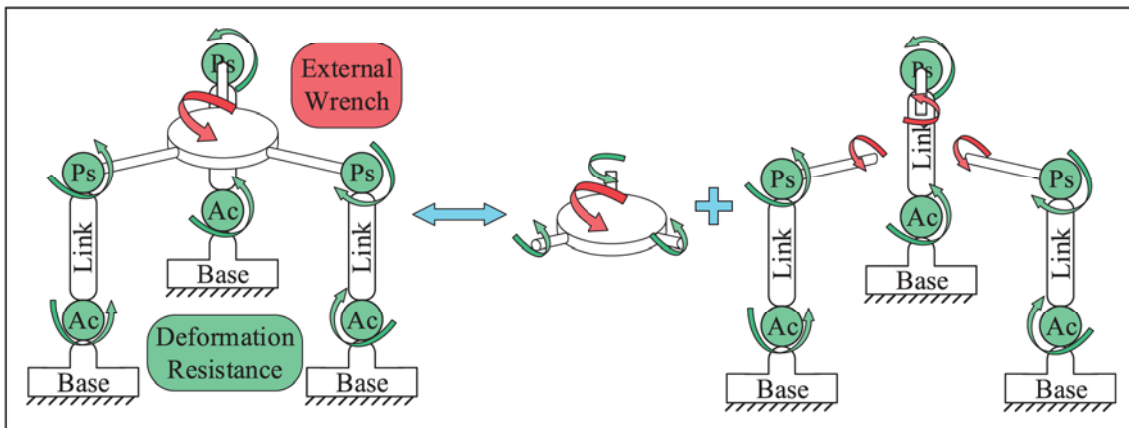

Figure 1. Schematic drawing of the division of a parallel manipulator.

Jacobian $\mathbf{J}_{F\eta i}$ according to the duality. However, if passive joints on the branch satisfies

$$\mathbf{J}_{\vartheta i}^{\mathrm{T}}\mathbf{J}_{\eta i} \neq O \tag{18}$$

then there always has

$$\exists \delta\vec{\vartheta}_i \neq \vec{0} \in \Omega_{\vartheta i}, \delta\vec{\eta}_i \neq \vec{0} \in \Omega_{\eta i} : \\ \delta\vec{\vartheta}_i^{\mathrm{T}}\mathbf{J}_{\vartheta i}^{\mathrm{T}}\mathbf{J}_{\eta i}\delta\vec{\eta}_i = \vec{\xi}_{\vartheta i}^{\mathrm{T}}\vec{\xi}_{\eta i} \neq 0 \tag{19}$$

where

$$\vec{\xi}_{\vartheta i}^{\mathrm{T}} \neq \vec{0} \in \Omega_{C\vartheta i}, \vec{\xi}_{\eta i} \neq \vec{0} \in \Omega_{C\eta i} \tag{20}$$

where $\Omega_{C\vartheta i}$ represents the subspace of Ω_C and also the codomain of linear transformation $\mathbf{J}_{\vartheta i}$. As a result, there must be some non-zero wrenches on subspace $\Omega_{C\vartheta i}$ that makes the serial chain can't be in static equilibrium

$$\exists \vec{\tau}_i \neq \vec{0} \in \Omega_{C\vartheta i}, \delta\vec{q} \neq \vec{0} \in \Omega_{C\eta i} : \vec{\tau}_i^{\mathrm{T}}\delta\vec{q} \neq 0 \tag{21}$$

Therefore, to fulfil the condition of being in static equilibrium, the external wrench $\vec{\tau}_i$ acted on the branch chain can't be the arbitrary element of $\Omega_{C\vartheta i}$ while must be the element of its subspace

$$\Omega_{Cai} = \left\{ \vec{\xi} \in \Omega_C | \vec{\xi} \in \Omega_{C\vartheta i}; \; \vec{\xi}^{\mathrm{T}}\delta\vec{q} = 0, \forall \delta\vec{q} \in \Omega_{C\eta i} \right\} \tag{22}$$

and elements on the subspace of $\Omega_{\vartheta i}$ whose image is $\Omega_{C\vartheta i} \cap \Omega_{C\eta i}$, i.e.

$$\Omega_{\vartheta f i} = \left\{ \delta\vec{\vartheta}_i \in \Omega_{\vartheta i} | \mathbf{J}_{\vartheta i}\delta\vec{\vartheta}_i \in \Omega_{C\vartheta i} \cap \Omega_{C\eta i} \right\} \tag{23}$$

is thus forbidden in practice, which results in that the vectors on $\Omega_{\vartheta f i}$ can't be projected onto Cartesian space. In terms of manipulator compliance, partial local compliance doesn't participate the holistic compliance since the passive joints. Instead, if equation (18) doesn't hold, the linear transformation that projects the compliance would still be complete considering that $\Omega_{C\vartheta i} \cap \Omega_{C\eta i} = \{\vec{0}\}$ or rather $\Omega_{Cai} = \Omega_{C\vartheta i}$. As a result, CCT is just $\mathbf{J}_{\vartheta i}\mathbf{C}_{\vartheta i}\mathbf{J}_{\vartheta i}^{\mathrm{T}}$ in this condition and it thus is drawn that the target transformation is equal to $\mathbf{J}_{\vartheta i}$ on Ω_{Cai}.

To sum up from the perspective of subspace analysis, if divide the linear transformation into two parts as shown in Figure 2(a), the part mapping from $\Omega_{\vartheta f i}$ is forbidden in order to keep the branch chain in static equilibrium, while only the part mapping to Ω_{Cai} is permissible and exactly the target transformation that determines the practical holistic stiffness of the manipulator. Describing the phenomenon in

visualizing words, the passive joints work like a "light shield", which partially shields the "light" (i.e., the linear transformation that projects the compliance) from $\Omega_{\vartheta i}$ to Ω_C. Therefore, the effect of passive joints on the holistic compliance of a manipulator is called "shielding effect" in this paper. In addition, in order to distinguish the observable holistic compliance tensor restricted to Ω_{Cai} from the complete holistic compliance tensor on $\Omega_{C\vartheta i}$, the former is called effective Cartesian space compliance tensor and the latter is called original Cartesian space compliance tensor in this paper.

To obtain the target transformation, one of the methods is to introduce an orthogonal projector. Denote the orthogonal complement of $\Omega_{C\eta i}$ as $\Omega_{C\eta i}^{\perp}$, and an orthogonal projector onto $\Omega_{C\eta i}^{\perp}$ is a linear transformation that satisfies

$$\begin{cases} \mathbf{P}_{\Omega_{C\eta i}^{\perp}}\vec{\xi} = \vec{\xi}, \; \forall \vec{\xi} \in \Omega_{C\eta i}^{\perp} \\ \mathbf{P}_{\Omega_{C\eta i}^{\perp}}\vec{\xi} = \vec{0}, \; \forall \vec{\xi} \in \Omega_{C\eta i} \end{cases} \tag{24}$$

where $\mathbf{P}_{\Omega_{C\eta i}^{\perp}}$ is the orthogonal projector. Obviously, according to expression (23), compound mapping $\mathbf{P}_{\Omega_{C\eta i}^{\perp}}\mathbf{J}_{\vartheta i}$ thus satisfies

$$\mathbf{P}_{\Omega_{C\eta i}^{\perp}}\mathbf{J}_{\vartheta i}\delta\vec{\vartheta}_i = \vec{0}, \; \forall \delta\vec{\vartheta}_i \in \Omega_{\vartheta f i} \tag{25}$$

In addition, considering that

$$\vec{\xi}^{\mathrm{T}}\delta\vec{q} = 0, \forall \delta\vec{q} \in \Omega_{C\eta i} \iff \vec{\xi} \in \Omega_{C\eta i}^{\perp} \tag{26}$$

we have

$$\Omega_{Cai} \subset \Omega_{C\eta i}^{\perp} \tag{27}$$

and thus

$$\mathbf{P}_{\Omega_{C\eta i}^{\perp}}\mathbf{J}_{\vartheta i}\delta\vec{\vartheta}_i = \mathbf{J}_{\vartheta i}\delta\vec{\vartheta}_i, \; \forall \delta\vec{\vartheta}_i \in \Omega_{\vartheta i} \text{ and } \delta\vec{\vartheta}_i \notin \Omega_{\vartheta f i} \tag{28}$$
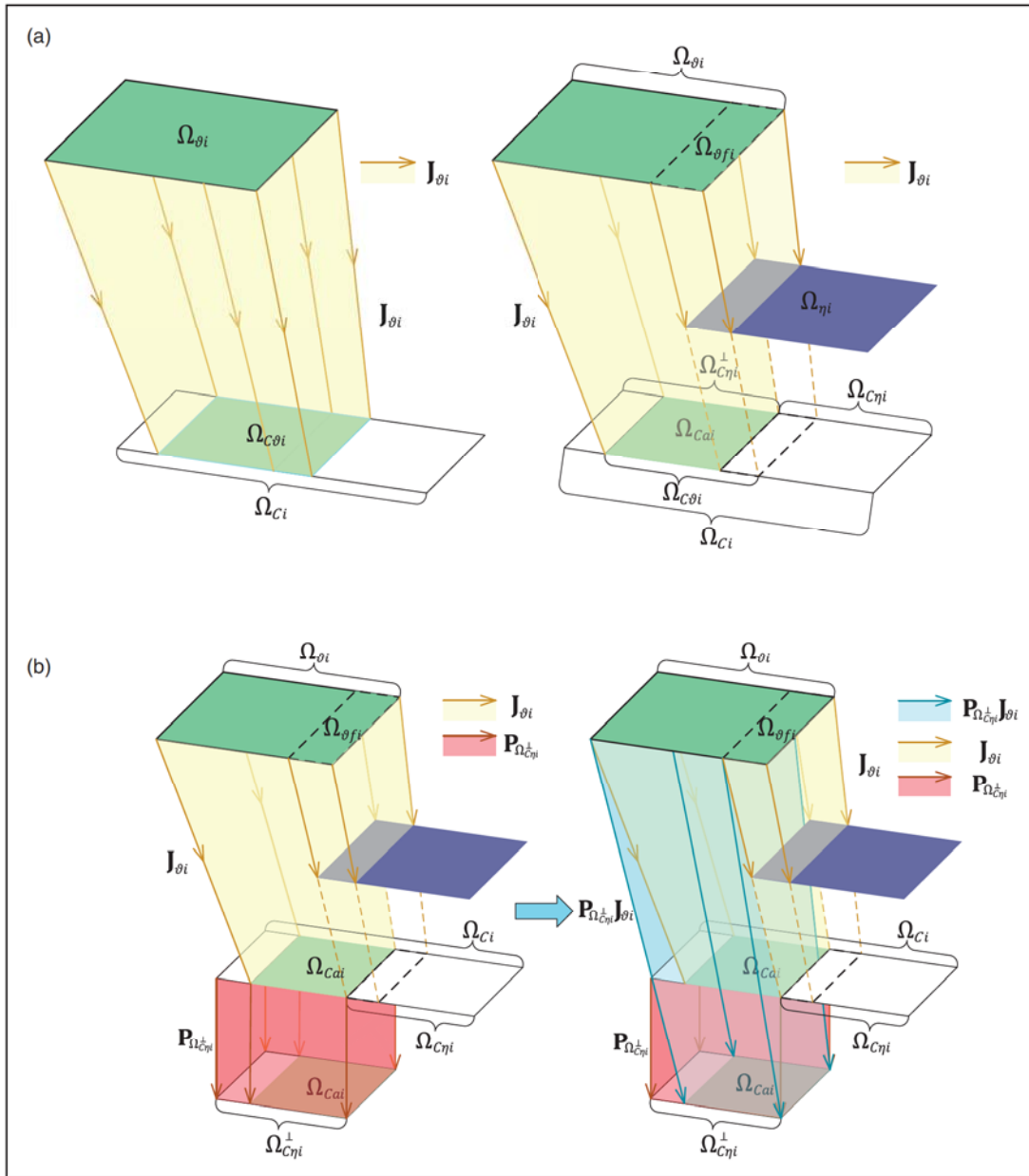
Obviously, the compound mapping $\mathbf{P}_{\Omega_{C\eta i}^{\perp}}\mathbf{J}_{\vartheta i}$ is exactly the target transformation as shown in Figure 2(b).

There are many ways to obtain $\mathbf{P}_{\Omega_{C\eta i}^{\perp}}$. First of all, $\mathbf{P}_{\Omega_{C\eta i}^{\perp}}$ could be indirectly obtained from transformation $\mathbf{J}_{\eta i}$. Considering that

$$\text{Range}(\mathbf{J}_{\eta i}) = \Omega_{C\eta i} \tag{29}$$

thus one of the orthogonal projectors onto subspace $\Omega_{C\eta i}$ is

$$\mathbf{P}_{C_{\eta i}} = \mathbf{J}_{\eta i}\left(\mathbf{J}_{\eta i}^{\mathrm{T}}\mathbf{J}_{\eta i}\right)^{-1}\mathbf{J}_{\eta i}^{\mathrm{T}} \tag{30}$$

Figure 2. Schematic drawing of proposed method: (a) schematic drawing of the effect of passive joints on the local compliance; (b) schematic drawing of the function of orthogonal projecting.

and

$$\mathbf{P}_{\Omega_{C\eta i}^{\perp}}$$

is thus

$$\mathbf{P}_{\Omega_{C\eta i}^{\perp}} = \mathbf{I}_6 - \mathbf{J}_{\eta i}\left(\mathbf{J}_{\eta i}^{\mathrm{T}}\mathbf{J}_{\eta i}\right)^{-1}\mathbf{J}_{\eta i}^{\mathrm{T}} \tag{31}$$

If $\mathbf{J}_{\eta i}$ is not a column full-rank matrix, the redundant columns could be taken out to get a column full rank matrix and simplify the calculation of the projector. Besides, comparing compound transformation

$\mathbf{P}_{\Omega_{C\eta i}^{\perp}}\mathbf{J}_{\vartheta i}$ with N in expression (15), it could be drawn that one of the possible forms of the constraint Jacobian matrix is that

$$G_{\eta\vartheta} = \left(\mathbf{J}_{\eta i}^{\mathrm{T}}\mathbf{J}_{\eta i}\right)^{-1}\mathbf{J}_{\eta i}^{\mathrm{T}}\mathbf{J}_{\vartheta i} \tag{32}$$

So all the required Jacobian matrix has been obtained.

In fact, if the rank of $\mathbf{J}_{\eta i}$ is larger than 3, there is a simpler method to obtain the orthogonal projector. Denote the singular value decomposition of $\mathbf{J}_{\eta i}$ as

$$\mathbf{J}_{\eta i} = \begin{bmatrix} \mathbf{U}_{i1} & \mathbf{U}_{i2} \end{bmatrix} \begin{bmatrix} \mathbf{\Sigma} & \\ & \mathbf{O} \end{bmatrix} \begin{bmatrix} \mathbf{V}_{i1}^{\mathrm{T}} \\ \mathbf{V}_{i2}^{\mathrm{T}} \end{bmatrix} = \mathbf{U}_{i1}\mathbf{\Sigma}\mathbf{V}_{i1}^{\mathrm{T}} \tag{33}$$

$$\mathbf{U}_{i1} = \begin{bmatrix} {}^{i}\vec{\mathbf{u}}_{1} & \cdots & {}^{i}\vec{\mathbf{u}}_{r} \end{bmatrix} \qquad (34)$$

$$\mathbf{U}_{i2} = \begin{bmatrix} {}^{i}\vec{\mathbf{u}}_{r+1} & \cdots & {}^{i}\vec{\mathbf{u}}_{6} \end{bmatrix} \qquad (35)$$

where r represent the rank of $\mathbf{J}_{\eta i}$. It is proved that ${}^{i}\vec{\mathbf{u}}_{1} \cdots {}^{i}\vec{\mathbf{u}}_{r}$ and ${}^{i}\vec{\mathbf{u}}_{r+1} \cdots {}^{i}\vec{\mathbf{u}}_{6}$ are respectively the orthonormal basis of $\Omega_{C\eta i}$ and $\Omega_{C\eta i}^{\perp}$ and thus the orthogonal projector onto subspace $\Omega_{C\eta i}^{\perp}$ is

$$\mathbf{P}_{\Omega_{C\eta i}^{\perp}} = \mathbf{U}_{i2}\left(\mathbf{U}_{i2}^{T}\mathbf{U}_{i2}\right)^{-1}\mathbf{U}_{i2}^{T} = \mathbf{U}_{i2}\mathbf{U}_{i2}^{T} \qquad (36)$$

In fact, singular value decomposition is not inevitable and orthogonal projectors could also be obtained by kinematic pair screw analysis. It is proved that the vector system corresponding to the constraint wrench system is just the basis of $\Omega_{C\eta i}^{\perp}$, and thus the projector $\mathbf{P}_{\Omega_{C\eta i}^{\perp}}$ can be directly obtained using equation (36). And it is always very convenient to analytically obtain the constraint wrench system if the matrix rank of $\mathbf{J}_{\eta i}$ is larger than 3. In a word, the method provides an open framework that any algebraic tools that could obtain the projector would be compatible, which make it possible to obtain a pithier model.

Now, the CCT of a serial chain could be expressed in an analytical form. Substitute the compound mapping $\mathbf{P}_{\Omega_{C\eta i}^{\perp}}\mathbf{J}_{\vartheta i}$ for the target transformation in CCT and the effective Cartesian space compliance tensor of a serial branch chain is obtained as

$$\mathbf{C}_{Ei} = \mathbf{U}_{i2}\mathbf{U}_{i2}^{T}\mathbf{J}_{\vartheta i}\mathbf{C}_{\vartheta i}\mathbf{J}_{\vartheta i}^{T}\mathbf{U}_{i2}\mathbf{U}_{i2}^{T} = \mathbf{U}_{i2}\mathbf{U}_{i2}^{T}\mathbf{C}_{ci}\mathbf{U}_{i2}\mathbf{U}_{i2}^{T} \qquad (37)$$

or

$$\mathbf{C}_{Ei} = \left(\mathbf{I}_{6} - \mathbf{J}_{\eta i}\left(\mathbf{J}_{\eta i}^{T}\mathbf{J}_{\eta i}\right)^{-1}\mathbf{J}_{\eta i}^{T}\right)$$
$$\mathbf{C}_{ci}\left(\mathbf{I}_{6} - \mathbf{J}_{\eta i}\left(\mathbf{J}_{\eta i}^{T}\mathbf{J}_{\eta i}\right)^{-1}\mathbf{J}_{\eta i}^{T}\right)^{T} \qquad (38)$$

where $\mathbf{C}_{ci}$ is the original Cartesian space compliance tensor which is obtained using $\mathbf{J}_{\vartheta i}\mathbf{C}_{\vartheta i}\mathbf{J}_{\vartheta i}^{T}$. Before obtaining the stiffness, it should be noted that the appropriate relationship between a stiffness tensor and the corresponding compliance tensor is that they are the Moore–Pseudoinverse of each other. The definition could be compatible even the condition that the stiffness tensor is non-full-rank. Therefore, EST of a serial branch chain is

$$\mathbf{K}_{Ei} = \left(\mathbf{U}_{i2}\mathbf{U}_{i2}^{T}\mathbf{C}_{ci}\mathbf{U}_{i2}\mathbf{U}_{i2}^{T}\right)^{\dagger} = \mathbf{U}_{i2}\left(\mathbf{U}_{i2}^{T}\mathbf{C}_{ci}\mathbf{U}_{i2}\right)^{\dagger}\mathbf{U}_{i2}^{T} \qquad (39)$$

where "$\dagger$" represents the Moore–Penrose pseudoinverse of a compliance tensor $\mathbf{C}_{ci}$. It is seen that the acquisition of all the Jacobian matrices frees from the number and form of virtual joints and thus the virtual joints of arbitrary form and the number could be integrated into the VJM model. It is also seen that the dimensions of the matrix to be inversed are 6-x (x represents the matrix rank of $\mathbf{J}_{\eta i}$). By comparison, VJM in various studies[11,25–27] have to obtain the partition inversion of an augment matrix to acquire $\mathbf{K}_{Ei}$, i.e.

$$\begin{bmatrix} \mathbf{K}_{Ei} & * \\ * & * \end{bmatrix} = \begin{bmatrix} \mathbf{C}_{ci} & \mathbf{J}_{\eta i} \\ \mathbf{J}_{\eta i}^{T} & O \end{bmatrix}^{-1} \qquad (40)$$

Obviously, the dimension of the augment matrix is $6+y$ (y represents the number of column number of $\mathbf{J}_{\eta i}$) and more than that of proposed method. Besides, numeric solution would be necessary for VJM based on augment matrix to obtain $\mathbf{K}_{Ei}$ since $\mathbf{C}_{ci}$ is usually singular and $\mathbf{J}_{\eta i}$ is not square matrix. In other words, proposed method has a higher computation efficiency.

Substitute equation (239) for the $\mathbf{K}_{i}$ in equation (16), and the holistic stiffness of a parallel manipulator is

$$\mathbf{K}_{M} = \sum_{i=1}^{n}\mathbf{U}_{2i}\left(\mathbf{U}_{2i}^{T}\mathbf{J}_{\vartheta i}\mathbf{C}_{\vartheta i}\mathbf{J}_{\vartheta i}^{T}\mathbf{U}_{2i}\right)^{\dagger}\mathbf{U}_{2i}^{T} \qquad (41)$$

The formulas have explicit and analytical forms and thus could be directly computed, which is beneficial to optimizations. Considering that there are no special restrictions on the number of branch chain, the formula could be applied to an under, complete or over constraints manipulator.

Extension of proposed method

If considering the preloads on the manipulator, the VJM formula of a parallel manipulator should be modified according to equation (14)

$$\mathbf{K}_{M} = \sum_{i=1}^{n}\mathbf{K}_{Ei}\left[\mathbf{I}_{6} - \left(\vec{\tau}_{i}^{T} \otimes \mathbf{U}_{2i}\mathbf{U}_{2i}^{T}\mathbf{J}_{\vartheta i}\mathbf{C}_{\vartheta i}\right)\mathbf{H}_{Ni}\right] \qquad (42)$$

where the Hessian matrix of the i-th chain $\mathbf{H}_{Ni}(i = 1, \ldots, n)$ could be directly obtained using the Jacobian matrix of analytical form expressed in equation (31) or (36)

$$\mathbf{H}_{Ni} = \frac{\partial \text{vec}(N_{i}^{T})}{\partial \vec{q}^{T}} = \frac{\partial \text{vec}\left(\mathbf{J}_{\vartheta i}^{T}\mathbf{P}_{\Omega_{C\eta i}^{\perp}}\right)}{\partial \vec{q}^{T}}, \quad (i = 1, \ldots, n) \qquad (43)$$

The core problem left is to determine $\vec{\tau}_i\,(i=1,\ldots,n)$ and it would vary according to the types of the parallel manipulator.

When it comes to an under or complete constraint manipulator, there is always not internal wrench and any external wrench could be expressed as the sum of a unique set of $\vec{\tau}_i\,(i=1,\ldots,n)$ when the manipulator is in the equilibrium. From the perspective of subspace analysis, the statement is equivalent to

$$\Omega_t = \Omega_{Ca1}\oplus\Omega_{Ca2}\cdots\oplus\Omega_{Cai}\cdots\oplus\Omega_{Can} \tag{44}$$

where Ω_t represents the permissible space of external wrench and

$$\vec{t}\in\Omega_t;\;\vec{\tau}_i\in\Omega_{Cai},\;(i=1,\cdots,n) \tag{45}$$

In addition, the vector system $^1\vec{\mathbf{u}}_{r+1}\;\cdots$ $^1\vec{\mathbf{u}}_6\cdots{}^n\vec{\mathbf{u}}_6$ must be the basis of Ω_t since the vector system $^i\vec{\mathbf{u}}_{r+1}\;\cdots\;{}^i\vec{\mathbf{u}}_6,(i=1,\cdots,n)$ is the basis of $\Omega_{Cai},(i=1,\cdots,n).$As a result, the $\vec{\tau}_i\,(i=1,\cdots,n)$ could be directly determined using the oblique projector onto $\Omega_{Cai},\;(i=1,\cdots,n)$

$$\vec{\tau}_i = P_{\Omega_{Cai}}\vec{t} = \begin{bmatrix} O & \cdots & \mathbf{U}_{2i} & \cdots & O \end{bmatrix}$$
$$\begin{bmatrix} \mathbf{U}_{21} & \cdots & \mathbf{U}_{2n} \end{bmatrix}^{-1}\vec{t},\;(i=1,\cdots,n) \tag{46}$$

Matrix $\begin{bmatrix} \mathbf{U}_{21} & \cdots & \mathbf{U}_{2n} \end{bmatrix}$ could be extended to a full-rank matrix using arbitrary vectors linear independent from vector system $^1\vec{\mathbf{u}}_{r+1}\;\cdots\;{}^1\vec{\mathbf{u}}_6\;\cdots$ $^n\vec{\mathbf{u}}_6$ in the case of under constraint manipulators, at which $\Omega_t\neq\mathbb{R}^6$. And thus the Cartesian space stiffness of the parallel manipulator could be expressed as

$$\mathbf{K}_M = \sum_{i=1}^n \mathbf{K}_{Ei}\left[\mathbf{I}_6 - \left(\vec{t}^T P_{\Omega_{Cai}}^T \otimes \mathbf{U}_{2i}\mathbf{U}_{2i}^T\mathbf{J}_{\vartheta i}\mathbf{C}_{\vartheta i}\right)\mathbf{H}_{Ni}\right] \tag{47}$$

It is seen that the modified formula retains an explicit and analytical form and could also be directly computed, which is friendly to the optimization. However, things would be difficult when it comes to an overconstraint parallel manipulator. Although the introduction of the projectors could simplify the stiffness expression of each chain, it is still hard to obtain holistic stiffness formulas of explicit form and consequently the numeric iteration would be inevitable. Considering that the proportion of complete constraint manipulators is massive in practice, the proposed method would be still of great practical significance.

Application in the alignment mechanism

China's large space telescope is one of the most significant ongoing scientific projects, whose weight is expected more than 15,000 kg, diameter of the primary mirror is 2 m, optical resolution is comparable to that of Hubble Space Telescope (HST) and field of vision is 300 times that of the HST. The scientific mission of the telescope is to survey the formation and evolution of celestial bodies, detect dark matter and reconstruct early universe density perturbation. The function of the alignment mechanism is to maneuver on large scale so that the telescope could switch in multiple observation modes. Therefore, the kinematics of the alignment mechanism has been researched.[33] Besides, it should also provide sufficiently rigid support for the optical payload in order to ensure the optical system in good condition in orbit and additionally the safety of the payload during launch. The performance index of the support is the first-order mode frequency of the combined system consisting of the alignment mechanism and optical payload. However, the vibration characteristics of the combined system could be estimated using the inertia of the payload and stiffness of the support according to the preliminary tests. As a result, holistic stiffness of the alignment is of great importance and this subsection would introduce the application of the proposed method to obtain an analytical stiffness model for optimizations.

VJM model of the parallel alignment mechanism

The specific structure of the alignment mechanism in China's large space telescope is shown in Figure 3(a) and (b). There are three main parts, namely the base, six legs and payload platform. The base is fixed on the truss structure of the telescope while the payload platform is installed with the optical payload and the legs support the platform. The preliminary tests showed that the first six order mode frequencies that computed using the inertia parameters of the payload and the holistic static stiffness of the alignment mechanism are well consistent with the FEM results, which is considered as the result of the high-stiffness of payload as well as that the movable mass of combined system mainly concentrates on the payload. Therefore, the optimization of the alignment mechanism as an independent module could take holistic static stiffness as the objective.

The static stiffness of the alignment could be modelled using the proposed method. First of all, the parallel mechanism is divided into six serial branch chains that consist of part of the base, actuators, eccentric dual revolute joints and part of the platform. There are five motion DOF of passive joints and one motion DOF of actuator on each branch chain. Obviously, the parallel mechanism is a complete constraint mechanism and thus the internal force could be left out of account and external wrench distributed to each branch chain could be obtained using projectors. Considering that motion DOF of passive joints is larger than 3, the method
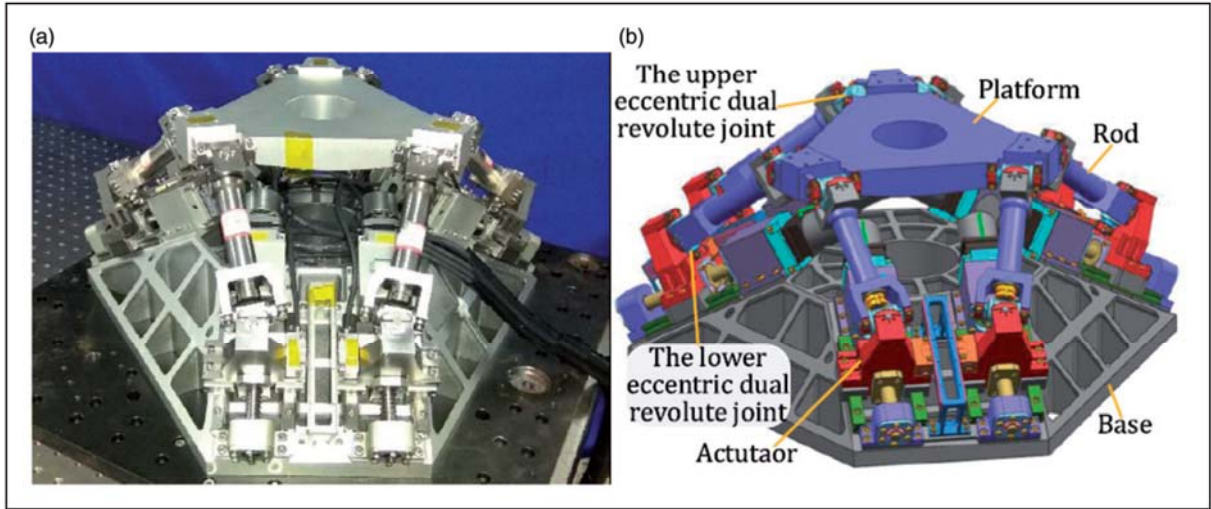
Figure 3. The prototype of the alignment mechanism: (a) 3D model; (b) the entity.

based on the kinematic screw analysis would be adopted here to obtain matrix $\mathbf{U}_{2i}(i = 1, \ldots, 6)$.

Take the i-th branch chain as an example (as shown in Figure 4), the form of equivalent kinematic pair screw system of passive joints can be expressed as
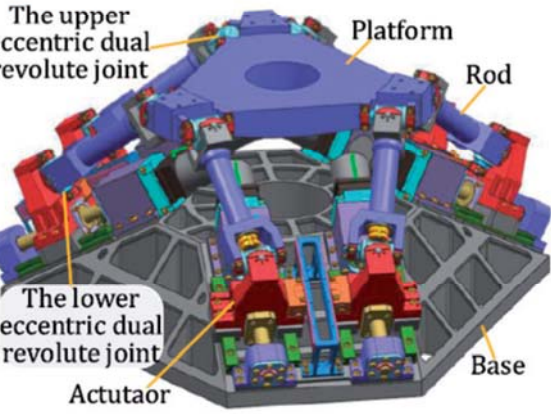
$$
\begin{cases}
\$_{i1} = \left(-\mathcal{C}_{\eta_{i2}} \mathcal{S}_{\eta_{i3}} \mathcal{C}_{\eta_{i2}} \mathcal{C}_{\eta_{i3}} \mathcal{S}_{\eta_{i2}}; h_{i1} \mathcal{C}_{\eta_{i2}} \mathcal{C}_{\eta_{i2}} h_{i1} \mathcal{C}_{\eta_{i2}} \mathcal{S}_{\eta_{i3}} 0 \right) \\
\$_{i2} = \left(\mathcal{C}_{\eta_{i3}} \quad \mathcal{S}_{\eta_{i3}} \quad 0; \quad 0 \quad 0 \quad 0 \right) \\
\$_{i3} = \left(0 \quad 0 \quad 1; \quad 0 \quad 0 \quad 0 \right) \\
\$_{i4} = \left(0 \quad 1 \quad 0; \quad h_{i2} \quad 0 \quad 0 \right) \\
\$_{i5} = \left(\mathcal{C}_{\eta_{i4}} \quad 0 \quad -\mathcal{S}_{\eta_{i4}}; \quad 0 \quad h_{i2} + h_{i3}\mathcal{C}_{\eta_{i4}} 0 \right)
\end{cases}
$$
$$(48)$$

where $\mathcal{C}_{(\cdot)}$ and $\mathcal{S}_{(\cdot)}$ respectively represent sine and cosine, and the definition of the parameters could be found in Figure 4. Observing the kinematic screw system, it is obvious that one of the constraint wrenches of the i-th branch chain is

$$
\$_i^c = \left(\vec{n}_i^{\mathrm{T}}; \quad (\vec{r}_i \times \vec{n}_i)^{\mathrm{T}} \right)
$$
$$
= (0 \quad 0 \quad 1; \quad 0 \quad 0 \quad 0), \quad (i = 1, \ldots, 6) \quad (49)
$$

where $\vec{n}_i$ and $\vec{r}_i$ respectively represent the direction of the i-th rod and the position vector of a point on the central axe of the i-th rod which could be arbitrarily chosen. The left part of the formula (49) depends only on the topology of the chain and thus holds whatever the definition of coordinate system are. In addition, considering that five twists of the kinematic screw system are always linear independent, the rank of the constraint wrench system is 1 and thus matrix $\mathbf{U}_{2i}$ is expressed as

$$
\mathbf{U}_{2i} = \frac{1}{\left(\begin{array}{c} \vec{n}_i \\ \vec{r}_i \times \vec{n}_i \end{array} \right)} \left(\begin{array}{c} \vec{n}_i \\ \vec{r}_i \times \vec{n}_i \end{array} \right)
$$
$$
= \frac{1}{\|\vec{\zeta}_i\|} \vec{\zeta}_i, \quad (i = 1, \ldots, 6) \quad (50)
$$

Therefore, according to equation (40), the CCT of the alignment mechanism is thus expressed as

$$
\mathbf{K}_{cE} = \sum_{i=1}^{6} \mathbf{U}_{2i} \left(\mathbf{U}_{2i}^{\mathrm{T}} \mathbf{J}_{\vartheta i} \mathbf{C}_{\vartheta i} \mathbf{J}_{\vartheta i}^{\mathrm{T}} \mathbf{U}_{2i} \right)^{\dagger} \mathbf{U}_{2i}^{\mathrm{T}}
$$
$$
= \sum_{i=1}^{6} \frac{\vec{\zeta}_i \vec{\zeta}_i^{\mathrm{T}}}{\vec{\zeta}_i^{\mathrm{T}} \mathbf{J}_{\vartheta i} \mathbf{C}_{\vartheta i} \mathbf{J}_{\vartheta i}^{\mathrm{T}} \vec{\zeta}_i} \quad (51)
$$

The formula (51) could be applied to model the stiffness of alignment mechanism when it works in orbit. However, it is necessary to consider the preload on the mechanism in the case of ground test and the formula of holistic stiffness is modified as

$$
\mathbf{K}_{cE} = \sum_{i=1}^{6} \frac{\vec{\zeta}_i \vec{\zeta}_i^{\mathrm{T}}}{\vec{\zeta}_i^{\mathrm{T}} \mathbf{J}_{\vartheta i} \mathbf{C}_{\vartheta i} \mathbf{J}_{\vartheta i}^{\mathrm{T}} \vec{\zeta}_i}
$$
$$
\left[\mathbf{I}_6 - \left(\vec{r}^{\mathrm{T}} P_{\Omega_{Cai}}^{\mathrm{T}} \otimes \vec{\zeta}_i \vec{\zeta}_i^{\mathrm{T}} \mathbf{J}_{\vartheta i} \mathbf{C}_{\vartheta i} \right) \mathbf{H}_{Ni} \right] \quad (52)
$$

where

$$
\mathbf{H}_{Ni} = \frac{\partial \mathrm{vec} \left(\mathbf{J}_{\vartheta i}^{\mathrm{T}} \vec{\zeta}_i \vec{\zeta}_i^{\mathrm{T}} \right)}{\partial \vec{q}^{\mathrm{T}}}
$$
$$
= \frac{\partial \mathrm{vec} \left(\mathbf{J}_{\vartheta i}^{\mathrm{T}} \vec{\zeta}_i \vec{\zeta}_i^{\mathrm{T}} \right)}{\partial \vec{\vartheta}_i^{\mathrm{T}}} \frac{\vec{\zeta}_i \vec{\zeta}_i}{\vec{\zeta}_i^{\mathrm{T}} \vec{\zeta}_i} \mathbf{J}_{\vartheta i}^{\dagger \mathrm{T}}, \quad (i = 1, \cdots, 6)
$$
$$(53)$$

$$
P_{\Omega_{Cai}} = \left[\vec{0} \quad \cdots \quad \vec{\zeta}_i \quad \cdots \quad \vec{0} \right] \left[\vec{\zeta}_1 \quad \cdots \quad \vec{\zeta}_6 \right]^{-1},
$$
$$
(i = 1, \ldots, 6) \quad (54)
$$

It is seen that the analytical form of the VJM model of the alignment mechanism is simply obtained using the proposed method. Then all that is left is to obtain the local compliance attributes. In order to
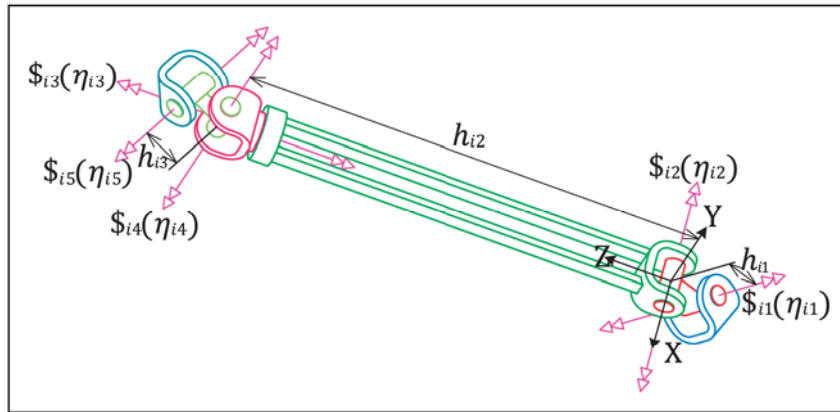
Figure 4. Schematic drawing of the screw analysis of a branch chain.

achieve comprehensive optimization of configuration parameters, all the possible deformations of each part should be considered. All the elastic parameters are obtained from virtual experiments in a finite element environment[19] and the results are shown in Table 2 in the Appendix. Meanwhile, the stiffness of the base is considered together with the actuators. The compliance distribution would alter after virtual joints are added to the alignment mechanism and relevant schematic drawings is shown in Figure 5(b).

Model verification

Because of the limited experimental condition, it is improper to carry out static tests on the prototype. And based on the engineering demand, the dynamic method would be adopted to verify the obtained VJM model instead, which would take the mode frequencies as a kind of convenient index of the holistic static stiffness characteristics. Considering that all the compliance parameters are obtained from finite element (FE) model, it is necessary to ensure the verification of FE model before verifying the VJM model and thus the virtual dynamic experiments were also carried out.

To simulate the combined system, a simulated payload of 32.1 kg is installed on the payload platform and by contrast, the total mass of all the remainder moving parts (not include payload platform) is only 2.031 kg. Therefore, the vibration characteristics of the simulated combined system consisting of simulated payload and the alignment mechanism could be estimated in the same manner. The total inertia matrix of the simulated payload and platform is measured form 3 D model and all the mass information are shown in Table 3 in the Appendix.

On the other hand, the influence is neglected in the subsection given the small damping ratios of a mechanical system. Therefore, the mode frequencies of vibration system approximate mode

poles and the modal estimation equation can be simplified as

$$\left(-\omega_i^2 \mathbf{M}_p + \mathbf{K}\right)\vec{v}_i = \vec{0}, \quad (i = 1,2\cdots 6) \tag{55}$$

where $\mathbf{K}$ is the holistic compliance matrix of the alignment mechanism and is $\mathbf{M}_p$ the total inertia matrix of the payload and the platform. Considering that two matrices in equation (55) should express in the same coordinate system., $\mathbf{M}_p$ should be transformed when the orientation of the payload platform changes

$$\mathbf{M}_p = \begin{bmatrix} \mathbf{R} & O \\ O & \mathbf{R} \end{bmatrix} \mathbf{M}_{p0} \begin{bmatrix} \mathbf{R}^{\mathrm{T}} & O \\ O & \mathbf{R}^{\mathrm{T}} \end{bmatrix} \tag{56}$$

where $\mathbf{M}_{p0}$ is the inertia matrix in the platform-fixed coordinate system that is same as the inertia system when the mechanism is in its original pose, and $\mathbf{R}$ is the coordinate transformation matrix from inertia system to platform-fixed coordinate system. In addition, there would be an external wrench on the alignment mechanism during the experiment, which mainly coming from the gravity of simulated payload and could be approximated as

$$\vec{t} = \begin{pmatrix} m\vec{g} \\ \vec{r}_e \times m\vec{g} \end{pmatrix} \tag{57}$$

where $\vec{g}$ represents the vector of gravitational acceleration, and m is the total mass of the combined system of the platform and the simulated payload, and $\vec{r}_e$ is the position vector of the centroid of the combined system.

The experimental arrangement used to obtain the mode frequencies is shown in Figure 6. The hammer (Dytran Instruments, Inc., 11.466 mV/N) was equipped with a rubber tip is used to knock the vibration system at different points in order to only and fully excite the six lowest modals, and the excitation
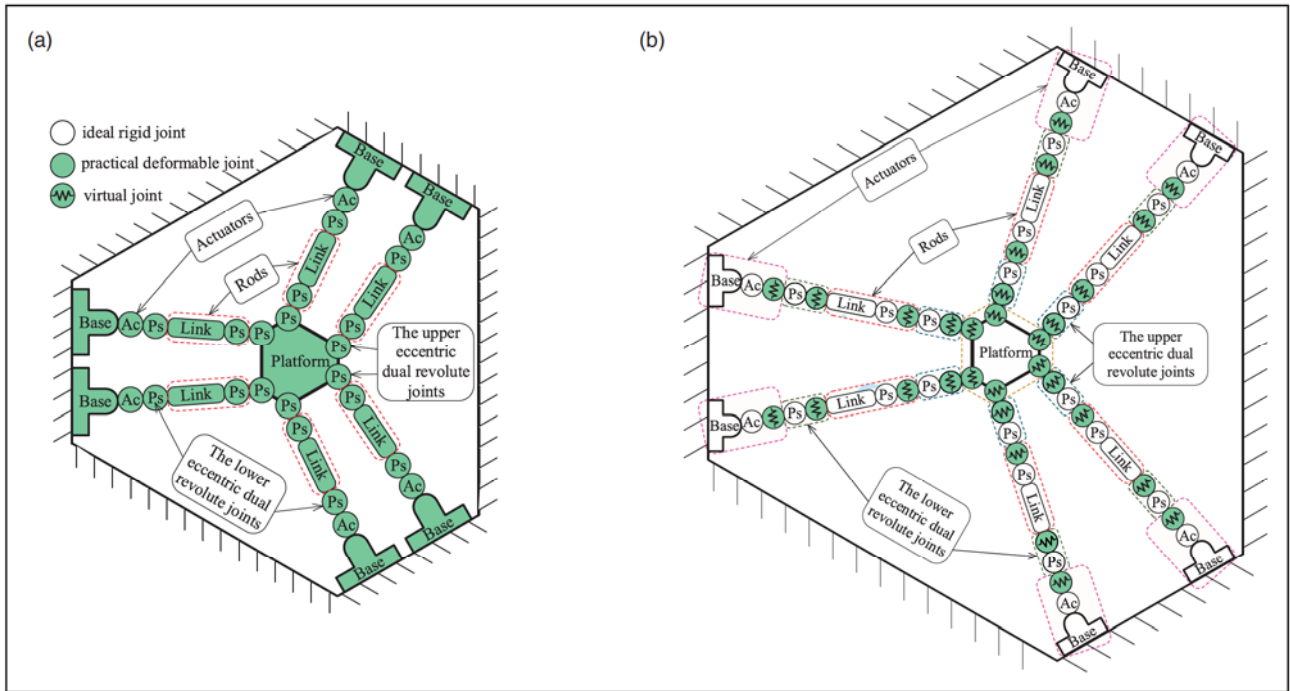
Figure 5. Topological schematic drawing of the prototype: (a) schematic drawing of the original compliance distribution; (b) schematic drawing of VJM model.
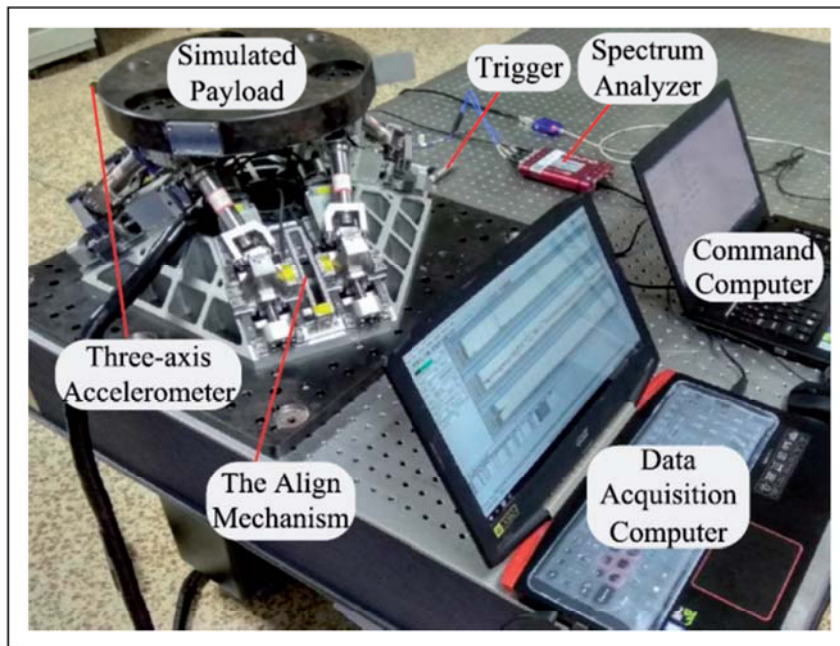
**Figure 6.** Test configuration of the mode frequencies.

signals and response information are acquired by the piezoelectric sensor in the trigger and the triaxial accelerometer (PCB Piezotronics, Inc., X:990 mV/g, Y:1048 mV/g, Z:1006 mV/g) on the platform. Sensor data are then transmitted to the computer through the multi-channel spectrum analyzer (DataPhysics Instruments GmbH, max 20 kHz, 24 bit, 10 V). Then the mode frequencies and damping ratios are obtained by modal analysis. After measurement of

the six lowest mode frequencies in a given pose, the alignment mechanism transfers to the next given pose for a new measurement.

The damping ratio of each mode pole is shown in Table 1, and it's drawn that the damping ratio of each pole does not exceed 3% and thus equation (55) holds. Then mode frequencies measured from the experiments and those obtained from the FEM and VJM model are shown in Figure 7(a) to (d). It could

Table 1. Damping ratio of each modal pole of the combined system.

Modal order	1st	2nd	3rd	4th	5th	6th
(0°, 0°, 0°)	1.00%	1.16%	1.48%	1.34%	1.86%	1.64%
(0°, 4.5°, 0°)	2.28%	1.98%	1.72%	1.99%	1.59%	1.63%
(7.7°, −2°, 0°)	2.67%	1.91%	2.47%	1.72%	1.02%	1.26%
(9°, 0°, 0°)	2.43%	1.67%	1.86%	1.60%	1.60%	1.94%
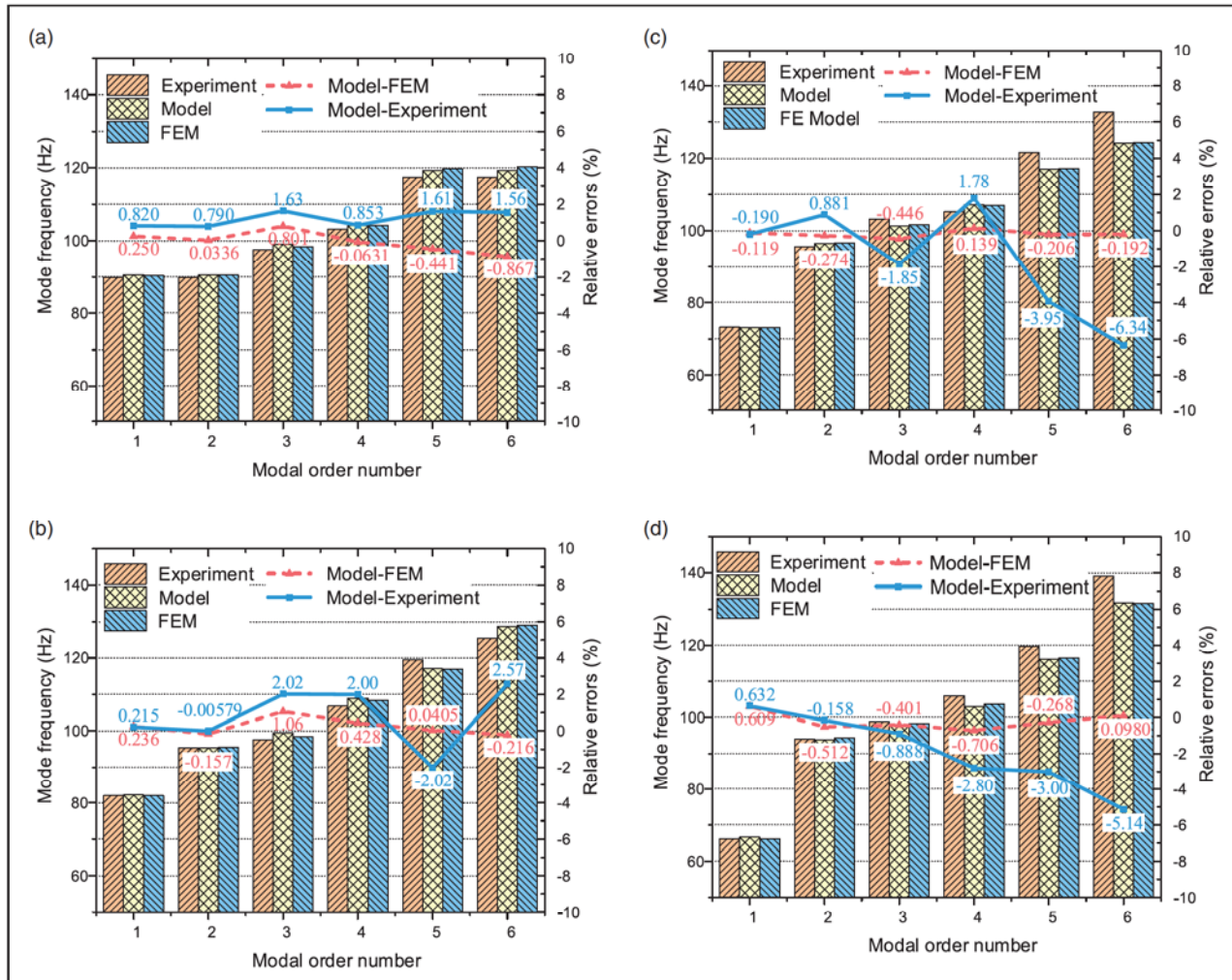
Figure 7. Mode frequencies results of the prototype: (a) the results when the platform is at the original position; (b) the results when the RPY coordinates of the platform are (0°, 4.5°, 0°); (c) the results when the RPY coordinates of the platform are (7.7°, −2°, 0°); (d) the results when the RPY coordinates of the platform are (9°, 0°, 0°).

be drawn that the distribution of mode frequencies derived from the VJM model is basically consistent with that from FEM, and the relative errors do not exceed 1.5%. Considering that direct comparison results between the VJM model and experiments do not exceed 7%, therefore, obtained VJM model can be considered valid and be applied for the subsequent optimization design of configuration parameters.

Conclusion

Oriented towards parameter optimization of parallel manipulators, the paper introduced a virtual joint method based on subspace analysis, which allows the models of analytical form and high computational efficiency. From the perspective of subspace, the "shielding effect" of passive joints on the local stiffness was revealed and the concept of EST was brought forward. Then the orthogonal projector was introduced to obtain the EST, which allows the formulas of analytical form and provides an open framework that is compatible with more numbers of convenient algebraic tools. Meanwhile, the dimensions of the matrix inversions are always limited to no more than 6 and the more the number of passive DOF, the less of the dimension of the matrix to be

inversed, which is less than $6 + x$ and thus leads to higher computation efficiency. Based on the general formulas of VJM, the method was also generalized to the case of parallel mechanisms under preloads while retaining the analytical form. Proposed method was applied to the prototype of the alignment mechanism in China's large space telescope and results of dynamic experiments showed that maximum relative errors between the first six order mode frequencies derived from obtained VJM model and those obtained from experiments was less than 7%, illustrating the validity of obtained model. The proposed method of projection is effective to model the stiffness of parallel manipulators with perfect passive joints and we are intending to model the stiffness of parallel manipulators with imperfect passive joints next.

Declaration of Conflicting Interests

The author(s) declared no potential conflicts of interest with respect to the research, authorship, and/or publication of this article.

Funding

ORCID iD

Hasiaoqier Han ⓘ https://orcid.org/0000-0002-8427-3377

References

1. Schipani P, D'Orsi S, Fierro D, et al. Active optics control of VST telescope secondary mirror. *Appl Opt* 2010; 49: 3199–3207.
2. Yue Z, Ye Y and Gu B. Modeling and simulation of a 6-DOF parallel platform for telescope secondary mirror. *SPIE*, 2014.
3. Yang Y, Zhen-Bang X, Chun-Yang H, et al. Design and testing of parallel alignment mechanism for space optical payload. In: *2nd Asia-Pacific conference on intelligent robot systems (ACIRS)*, 2017, pp. 254–258. New York: IEEE.
4. Ye Y, Yue Z and Gu B. ADRC control of a 6-DOF parallel manipulator for telescope secondary mirror. *J Instrum* 2017; 12: T03006–T03006.
5. Yun H, Liu L, Li Q, et al. Development of an isotropic Stewart platform for telescope secondary mirror. *Mech Syst Sig Process* 2019; 127: 328–344.
6. Li H and Hao G. Constraint-force-based approach of modelling compliant mechanisms: principle and application. *Precis Eng* 2017; 47: 158–181.
7. Klimchik A, Pashkevich A and Chablat D. Fundamentals of manipulator stiffness modeling using matrix structural analysis. *Mech Mach Theory* 2019; 133: 365–394.
8. Raoofian A, Taghvaeipour A and Kamali A. On the stiffness analysis of robotic manipulators and calculation of stiffness indices. *Mech Mach Theory* 2018; 130: 382–402.
9. Cammarata A. Unified formulation for the stiffness analysis of spatial mechanisms. *Mech Mach Theory* 2016; 105: 272–284.
10. Klimchik A, Pashkevich A and Chablat D. MSA-technique for stiffness modeling of manipulators with complex and hybrid structures. *IFAC-PapersOnLine* 2018; 51: 37–43.
11. Klimchik A, Chablat D and Pashkevich A. Stiffness modeling for perfect and non-perfect parallel manipulators under internal and external loadings. *Mech Mach Theory* 2014; 79: 1–28.
12. Salisbury JK. Active stiffness control of a manipulator in Cartesian coordinates. In: *Proceedings of the 19th IEEE conference on decision & control including the symposium on adaptive processes*, 1980, pp. 95–100. New York: IEEE.
13. Gosselin C. Stiffness mapping for parallel manipulators. *IEEE Trans Robot Automat* 1990; 6: 377–382.
14. Zhang D and Gosselin CM. Kinetostatic modeling of parallel mechanisms with a passive constraining leg and revolute actuators. *Mech Mach Theory* 2002; 37: 599–617.
15. Li Y and Xu Q. Stiffness analysis for a 3-PUU parallel kinematic machine. *Mech Mach Theory* 2008; 43: 186–200.
16. Kucuk S. Energy minimization for 3-RRR fully planar parallel manipulator using particle swarm optimization. *Mech Mach Theory* 2013; 62: 129–149.
17. Lian B, Sun T, Song Y, et al. Stiffness analysis and experiment of a novel 5-DoF parallel kinematic machine considering gravitational effects. *Int J Mach Tools Manuf* 2015; 95: 82–96.
18. Pigoski T, Griffis M and Duffy J. Stiffness mappings employing different frames of reference. *Mech Mach Theory* 1998; 33: 825–838.
19. Klimchik A, Pashkevich A and Chablat D. CAD-based approach for identification of elasto-static parameters of robotic manipulators. *Finite Elem Anal Des* 2013; 75: 19–30.
20. Klimchik A, Furet B, Caro S, et al. Identification of the manipulator stiffness model parameters in industrial environment. *Mech Mach Theory* 2015; 90: 1–22.
21. Kamali K and Bonev IA. Optimal experiment design for elasto-geometrical calibration of industrial robots. *IEEE/ASME Trans Mechatron* 2019; 24: 2733–2744.
22. Klimchik A, Ambiehl A, Garnier S, et al. Efficiency evaluation of robots in machining applications using industrial performance measure. *Robot Comput Integr Manuf* 2017; 48: 12–29.
23. Yang K, Yang W, Cheng G, et al. A new methodology for joint stiffness identification of heavy duty industrial robots with the counterbalancing system. *Robot Comput Integr Manuf* 2018; 53: 58–71.
24. Hoevenaars AG, Lambert P and Herder JL. Jacobian-based stiffness analysis method for parallel manipulators with non-redundant legs. *Proc IMechE, Part C: J Mechanical Engineering Science* 2016; 230: 341–352.
25. Sun T, Wu H, Lian B, et al. Stiffness modeling, analysis and evaluation of a 5 degree of freedom hybrid manipulator for friction stir welding. *Proc IMechE, Part C: J Mechanical Engineering Science* 2017; 231: 4441–4456.

26. Zhou G, Kim J and Je Choi Y. Jacobian approach to the kinestatic analysis of a full vehicle model with application to cornering motion analysis. *Proc IMechE, Part C: J Mechanical Engineering Science* 2020; 234: 3543–3559.
27. Chong Z, Hongwei G, Dan Z, et al. Stiffness modeling of n(3RRlS) reconfigurable series-parallel manipulators by combining virtual joint method and matrix structural analysis. *Mech Mach Theory* 2020; 152: 103960.
28. Görgülü İ, and and Dede MİC. Computation time efficient stiffness analysis of the modified R-CUBE mechanism. In: *Advances in Italian mechanism science, IFToMM ITALY 2018*. Cham: Springer International Publishing, 2019, pp. 231–239.
29. Görgülü İ, Carbone G and Dede MİC. Time efficient stiffness model computation for a parallel haptic

30. mechanism via the virtual joint method. *Mech Mach Theory* 2020; 143: 103614.
31. Yang J, Xu Z, Wu Q, et al. Dynamic modeling and control of a 6-DOF micro-vibration simulator. *Mech Mach Theory* 2016; 104: 350–369.
31. Wang X, Xu Z, He S, et al. Modeling and analysis of a multi-degree-of-freedom micro-vibration simulator. *Shock Vib* 2017; 2017: 1–17.
32. Wang XM, Xu ZB, Xia MY, et al. Research on a six-degree-of-freedom disturbance force and moment simulator for space micro-vibration experiments. *J Sound Vib* 2018; 432: 530–548.
33. Han H-s-a-q-e, Han C-Y, Xu Z-B, et al. Kinematics analysis and testing of novel 6-P-RR-R-RR parallel platform with offset RR-joints. *Proc IMechE, Part C: J Mechanical Engineering Science* 2019; 233: 3512–3530.

Appendix

Table 2. Total inertia matrix of simulated payload and platform.

Elements of the inertia matrix						Units	

$$
\begin{bmatrix}
33.23 & 0 & 0 & \vdots & 0 & -1.38 & -0.01 \\
0 & 33.23 & 0 & \vdots & 1.38 & 0 & 0.02 \\
0 & 0 & 33.23 & \vdots & 0.01 & -0.02 & 0 \\
\cdots & \cdots & \cdots & \vdots & \cdots & \cdots & \cdots \\
0 & 1.38 & 0.01 & \vdots & 0.32 & 0 & 0 \\
-1.38 & 0 & -0.02 & \vdots & 0 & 0.32 & 0 \\
-0.01 & 0.02 & 0 & \vdots & 0 & 0 & 0.51
\end{bmatrix}
\qquad
\begin{bmatrix}
kg & \vdots & kg \cdot m \\
\cdots & \vdots & \cdots \\
kg \cdot m & \vdots & kg \cdot m^2
\end{bmatrix}^{①}
$$

①.Units of the elements in the corresponding partition of the inertia matrix.

Table 3. Virtual elastic parameters obtained by adopting the FE method.

Component	Elastic parameters of virtual joint
Actuators	$\begin{bmatrix} 1.08\times10^5 & 4.33\times10^2 & 6.69\times10^4 & \vdots & 1.52\times10^4 & -7.31\times10^4 & 8.35\times10^3 \\ 4.33\times10^2 & 1.11\times10^5 & 4.27\times10^2 & \vdots & 1.14\times10^5 & 3.42\times10^4 & -2.83\times10^5 \\ 6.69\times10^4 & 4.27\times10^2 & 3.39\times10^5 & \vdots & 1.81\times10^4 & 1.61\times10^5 & -1.45\times10^4 \\ \cdots & \cdots & \cdots & \vdots & \cdots & \cdots & \cdots \\ 1.52\times10^4 & 1.14\times10^5 & 1.81\times10^4 & \vdots & 5.39\times10^7 & -2.2\times10^6 & 3.55\times10^6 \\ -7.31\times10^4 & 3.42\times10^4 & 1.61\times10^5 & \vdots & -2.2\times10^6 & 5.29\times10^7 & -4.75\times10^6 \\ 8.35\times10^3 & -2.83\times10^5 & -1.45\times10^4 & \vdots & 3.55\times10^6 & -4.75\times10^6 & 1.68\times10^7 \end{bmatrix}$
Eccentric dual revolute joints	$\begin{bmatrix} 5.37\times10^8 & -7.8\times10^7 & -2.49\times10^7 & \vdots & 7.72\times10^7 & 0. & 7.8\times10^5 \\ -7.8\times10^7 & 6.99\times10^8 & 8.71\times10^6 & \vdots & -3.39\times10^8 & 0. & -6.99\times10^6 \\ -2.49\times10^7 & 8.71\times10^6 & 7.85\times10^7 & \vdots & -8.35\times10^7 & 0. & -8.71\times10^4 \\ \cdots & \cdots & \cdots & \vdots & \cdots & \cdots & \cdots \\ 7.72\times10^7 & -3.39\times10^8 & -8.35\times10^7 & \vdots & 2.45\times10^8 & 0. & 3.39\times10^6 \\ 0. & 0. & 0. & \vdots & 0. & 0. & 0. \\ 7.8\times10^5 & -6.99\times10^6 & -8.71\times10^4 & \vdots & 3.39\times10^6 & 0. & 6.99\times10^4 \end{bmatrix}$
Rods	$\begin{bmatrix} 2.02\times10^8 & 4.88\times10^5 & 2.85\times10^6 & \vdots & 0. & -5.11\times10^7 & 3.29\times10^7 \\ 4.88\times10^5 & 2.09\times10^6 & -4.79\times10^4 & \vdots & 0. & 5.14\times10^6 & 6.83\times10^7 \\ 2.85\times10^6 & -4.79\times10^4 & 3.91\times10^6 & \vdots & 0. & -5.75\times10^7 & -1.6\times10^6 \\ \cdots & \cdots & \cdots & \vdots & \cdots & \cdots & \cdots \\ 0. & 0. & 0. & \vdots & 0. & 0. & 0. \\ -5.11\times10^7 & 5.14\times10^6 & -5.75\times10^7 & \vdots & 0. & 8.55\times10^8 & 1.68\times10^8 \\ 3.29\times10^7 & 6.83\times10^7 & -1.6\times10^6 & \vdots & 0. & 1.68\times10^8 & 2.24\times10^9 \end{bmatrix}$
Payload platform	$\begin{bmatrix} 1.57\times10^8 & -1.51\times10^8 & 2.67\times10^7 & \vdots & 6.18\times10^7 & -1.31\times10^8 & -2.86\times10^7 \\ -1.51\times10^8 & 3.55\times10^8 & -2.8\times10^7 & \vdots & 5.6\times10^6 & 1.69\times10^8 & -2.88\times10^8 \\ 2.67\times10^7 & -2.8\times10^7 & 2.83\times10^7 & \vdots & 7.52\times10^7 & 2.35\times10^7 & -9.62\times10^6 \\ \cdots & \cdots & \cdots & \vdots & \cdots & \cdots & \cdots \\ 6.18\times10^7 & 5.6\times10^6 & 7.52\times10^7 & \vdots & 2.25\times10^8 & 8.93\times10^7 & -1.32\times10^8 \\ -1.31\times10^8 & 1.69\times10^8 & 2.35\times10^7 & \vdots & 8.93\times10^7 & 2.09\times10^8 & -5.73\times10^7 \\ -2.86\times10^7 & -2.88\times10^8 & -9.62\times10^6 & \vdots & -1.32\times10^8 & -5.73\times10^7 & 4.81\times10^8 \end{bmatrix}$

Units of the elements in the corresponding partition of the parameter matrix are respectively.

$$\begin{bmatrix} \text{N/m} & \vdots & \text{N} \\ \cdots & \vdots & \cdots \\ \text{N} & \vdots & \text{N} \cdot \text{m/rad} \end{bmatrix}$$